Magnetic reconnection with QED effects in near-critical magnetic field

T. Grismayer,[1] K. M. Schoeffler,[1] L. O. Silva,[1] and D. Uzdensky[2,3]

[1] *GoLP/Instituto de Plasmas e Fusão Nuclear, Instituto Superior Técnico, Universidade de Lisboa, 1049-001 Lisboa, Portugal*

[2] *Center for Integrated Plasma Studies, Physics Department, University of Colorado, Boulder CO 80309, USA*

[3] *Institute for Advanced Study, 1 Einstein Dr., Princeton, NJ 08540, USA*

(Dated: May 9, 2017)

Magnetic reconnection in relativistic pair plasma with QED radiation and pair-creation effects in the presence of strong magnetic fields is investigated using 2D particle-in-cell simulations. This study is motivated by application to reconnection processes in extreme astrophysical environments around strongly magnetized neutron stars (e.g., magnetars), where the feedback of radiation due to the intense magnetic field on the emitting particles cannot be neglected, as it significantly modifies the dynamics of reconnection, the particle orbits, and the particle spectra. Unlike in traditional, non-radiative reconnection studies, a large portion of the initial magnetic energy in our strong-field simulations is converted into high-energy photons (X-rays and gamma-rays). Moreover in the most extreme case when the magnetic field approaches the critical Schwinger field, the production of energetic gamma-rays inside the magnetic islands eventually leads to the creation of secondary pairs. We would like to warn the reader that this numerical study is still a work in progress and that the results shown should not interpreted as definitive conclusions.

I. INTRODUCTION

Motivation

Magnetic reconnection is a fundamental plasma process involving a rapid change of magnetic topology and often leading to a violent release of magnetic energy. Most of the reconnection research has so far been driven to understand magnetic dissipation in space, solar, and laboratory plasmas. These environments are rather tenuous and hence are adequately described by traditional, low-energy-density plasma physics. However, magnetic reconnection is now also being increasingly recognized as an important physical process in numerous astrophysical contexts beyond the solar system, especially in relativistic high-energy astrophysics (pulsar magnetospheres, black-hole coronae and jets, magnetar flares in soft gamma repeaters, gamma-ray bursts). The magnetic energy density in many of these environments is so high that, when it is suddenly released through reconnection, the plasma is heated to ultra-relativistic temperatures. As a result, prompt radiative cooling often becomes important in these high-energy-density (HED) systems and governs the energy balance of the reconnection process [1].

In this study we will focus on the most extreme astrophysically relevant regime of reconnection involving magnetic fields approaching the critical quantum Schwinger magnetic field,

$$B_Q \equiv \frac{m_e^2 c^3}{\hbar e} = 4.4 \times 10^{13}\,\mathrm{G}, \tag{1}$$

possibly responsible for powering giant γ-ray flares in magnetospheres of magnetars [e.g., 2, 3]. The corresponding energy density is so high that its sudden release not only produces intense high-energy radiation but also feeds prodigious pair creation [3], resulting in a characteristic plasma density of order the Compton density

$$n_C = \lambda\!\!\!^{-}_C{}^{-3} = 1.739 \times 10^{31}\,\mathrm{cm}^{-3}, \tag{2}$$

where the reduced Compton length:

$$\lambda\!\!\!^{-}_C \equiv \frac{\hbar}{m_e c} = 3.86 \times 10^{-11}\,\mathrm{cm}. \tag{3}$$

Relevant QED processes

How magnetic reconnection takes place under these physical conditions is not yet understood, since rigorous investigation of this novel and so far unexplored reconnection regime requires taking into account various QED (Quantum

Electrodynamic) processes associated with strong magnetic fields. Many such processes can in principle take place but in this work we only consider two quantum processes that have highest probabilities. These processes are (1) single photon emission due to non-linear Compton scattering in intense electromagnetic fields (with self-consistent back-reaction recoil on the electron/positron), which is a QED extension of the classical synchrotron radiation; and (2) single-photon pair creation from the decay of hard gamma ray photons ($\hbar\omega > 2m_e c^2$) in intense electromagnetic fields, also known as the Breit-Wheeler pair production [4–8]. Other possible quantum processes such as the trident process, spontaneous pair production in vacuum, photon splitting and pair annihilation have substantially lower probability rates and therefore are omitted. The respective probability rates for photon emission and pair creation depend on the invariant quantum parameter χ and the energy of the particle. When the magnetic field dominates over the electrical field, a good approximation of the χ parameter is given by

$$\chi \simeq \frac{p_\perp}{m_e c}\frac{B}{B_Q}, \tag{4}$$

where $p_\perp$ is the particle momentum perpendicular to B. This parameter establishes a threshold at which QED effects becomes relevant. When $\chi > 1$, an electron has non-negligible probability of emitting a photon whose energy is comparable to that of the electron, and a hard gamma-ray photon has non-negligible probability of decaying into a pair (more details regarding the QED differential probability rate can be found in Appendix A). For values of $\chi < 1$, pair creation is exponentially suppressed but photon emission persists with constant photon rate (approximatively proportional to the local magnitude of the magnetic field) but with a radiated power that is reduced as χ decreases. When $\chi \ll 1$ the photon spectrum converges towards the classical synchrotron spectrum. In order to have χ values above unity, it is clear from Eq. (4) that one needs $p_\perp B/m_e c \gtrsim B_Q$, i.e., ultra-relativistic particles and strong magnetic fields. In large systems, where multiple magnetic island mergers occur, particles can get accelerated to very high energies producing non-thermal tails in energy spectra. Furthermore, in the absence of guide magnetic field, strong radiative cooling of the plasma in the plasmoids can cause significant compression, which can cause the magnetic field inside the plasmoids to rise well above the ambient (upstream) value. Thus, the ultra-relativistic particles generated in these tails while interacting with patches of intense magnetic fields can produce hard gamma-rays that may eventually decay into pairs.

II. CONDITIONS OF VALIDITY OF THE MODEL

The parameters needed to be specified for magnetic reconnection starting from a Harris sheet [9] equilibrium are the following: (A) ambient/background pair plasma parameters: the background electron/positron density n_b, the background temperature T_b, and the upstream (reconnecting) magnetic field B_0; (B) Initial current layer parameters: the electron density in the center of the Harris current sheet n_0, and the current half-thickness δ. Note, there is a minimum value $\delta = \delta_{cr}$ that can support a magnetic field B_0, for a given n_0. Also note that once n_0, B_0, and δ are specified, the remaining two Harris layer parameters, namely, the co-moving plasma temperature, T_H, and the drift velocity of the particles carrying the current in the layer, v_d, can be uniquely determined.

We will consider several physical assumptions of our model. Given the fundamental initial parameters T_b, n_b, and B_0 (or $\beta_{up} \equiv 16\pi n_b T_b/B_0^2$), we can show all the assumptions on one map in the 2D (n_b, T_b) parameter space. The requirements are the following:

- the density does not surpass the Compton density n_C;
- the electromagnetic fields are sub-critical ($E, B < B_Q$);
- discrete photon emission only occurs for ultra-relativistic particles;
- quasi-equilibrium (temperature does not cool significantly during the plasma crossing time of the system);
- quantum degeneracy effects can be neglected (temperature sufficiently large compared to the Fermi temperature);
- cyclotron orbits are not quantized (temperature sufficiently large compared to Landau energy levels);
- collective effects dominate (large Debye parameter);
- collisionless plasma (a typical particle does not collide during the plasma crossing time of the system).

The white region in Figure 1 corresponds to the parameter space where all our assumptions are satisfied. The most relevant constraints are the violet region, where the plasma rapidly cools, the green region, where collisions play an important role, and the pink region, where δ is too small to support the current associated with the magnetic field.

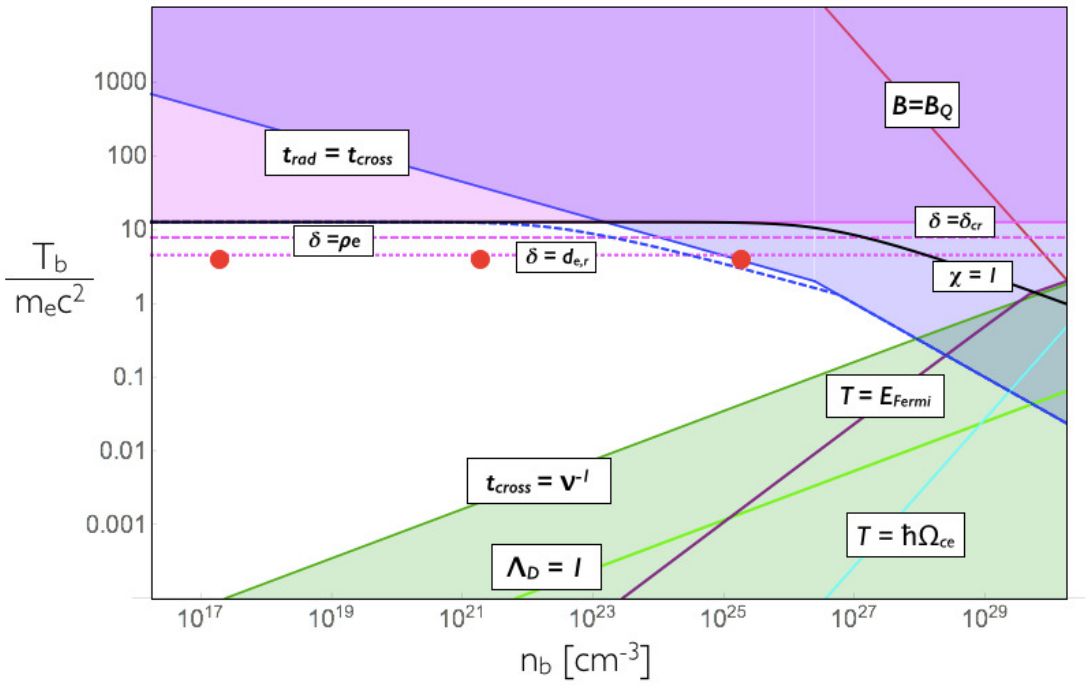

FIG. 1: T_b and n_b parameter space showing the various restrictions shown in Section II assuming $\delta/d_e = 4.49$, $n_b/n_0 = 0.1$, $t_{cross} = 2770\ \omega_p^{-1}$ [$10(3.3)L_y/c$ for $L_y/d_e = 277(831)$], and $\beta_{up} = 0.078$. Each simulation is represented by a red circle, each with $T_b/m_ec^2 = 4$. The dashed blue line represents the radiation limit for the Harris population as opposed to the background population shown in the solid blue line.

III. SIMULATIONS

Simulations setup

We investigate the QED effects on a relativistic reconnecting Harris current layer [10, 11] using 2D particle-in-cell (PIC) simulations with OSIRIS [12]. The QED version of OSIRIS has already been used to study the development of QED (electron-positron-photon) cascades in the laboratory with intense lasers [13, 14]. We use periodic boundary conditions, and initialize the distribution of magnetic field and density as a double Harris sheet, with a system size of $2L_x \times 2L_y$ ($-L_x < x < L_x$, $-L_y < y < L_y$). We begin with a Maxwell-Jüttner distribution of positrons and electrons in the Harris layer, and also include a background pair plasma at constant temperature. The density is normalized to n_0, time is normalized to the plasma frequency $\omega_p \equiv (4\pi n_0 e^2/m_e)^{1/2}$, distances are normalized to the electron inertial length $d_e \equiv c/\omega_p$, and the electromagnetic fields are normalized to $m_e c\omega_p/e$.

We have performed simulations varying the magnetic field strength B_0/B_Q, to compare systems with increasingly important effects of radiation, and in the most extreme case, QED. In doing this, we vary only n_0 keeping the normalized $B_0e/(m_ec\omega_p)$, T_b/m_ec^2, δ/d_e, and n_0/n_b, constant. The parameters of these simulations are shown in Table I, Table II, Table III. The parameters are chosen to lie in the white region of Fig. 1 and thus satisfy all our constraints, while run # 1 and # 4 reach the boundary where radiative cooling becomes significant ($t_{rad} \approx t_{cross}$).

TABLE I: Physical parameters.

T_b/m_ec^2	$B_0e/(m_ec\omega_p)$	σ_{up}	β_{up}	n_b/n_0	δ/d_e	T_H/m_ec^2	v_d/c	γ_d
4	4.53	205	0.078	0.1	4.49	6.91	0.56	1.21

($\sigma \equiv B_0^2/4\pi n_b m_e c^2$)

TABLE II: Numerical parameters.

L_x/d_e	L_y/d_e	grid	$\omega_p dt$	$\omega_p t_{max}$	ppc
277	277	640 × 640	0.5	2770	16
831	831	1920 × 1920	0.5	2770	16

TABLE III: Run parameters.

run	B_0/B_Q	B_0[Gauss]	$B_Q e/(m_e c\omega_p)$	n_b/n_C	n_b[cm^{-3}]	$L_x/d_e \times L_y/d_e$
1	4.5×10^{-3}	2.0×10^{11}	10^3	1.1×10^{-6}	1.9×10^{25}	277×277
2	4.5×10^{-5}	2.0×10^{9}	10^5	1.1×10^{-10}	1.9×10^{21}	277×277
3	4.5×10^{-7}	2.0×10^{7}	10^7	1.1×10^{-14}	1.9×10^{17}	277×277
4	4.5×10^{-3}	2.0×10^{11}	10^3	1.1×10^{-6}	1.9×10^{25}	831×831

Simulations results

In Fig. 2 we compare the evolution of energy partition for a fixed system size ($L_y/d_e = L_x/d_e = 277$), for several different values of B_0/B_Q. Fig. 1(a) (run #3, $B_0 = 2\times10^7$ G) corresponds to the case of relativistic reconnection where radiation is negligible. Close to half of the magnetic energy is transferred to particle kinetic energy. In Fig. 2(b) (run #2, $B_0 = 2\times10^9$ G) we can observe relativistic reconnection where radiation becomes relevant. Similar transfer of energy is shown, while oscillations between the magnetic and kinetic energy are damped. Only a small portion of the energy is radiated. In Fig. 2(c) (run #1, $B_0 = 2\times10^{11}$ G) we have relativistic reconnection with both QED and classical radiation. The magnetic energy is now converted predominantly to gamma rays, while the particle energy remains almost constant. In Fig. 2(a-b) particles are both heated and accelerated in the reconnection process, while in Fig. 2(c) particles effectively act as efficient radiators, rapidly converting the released energy into radiation via synchrotron cooling. Most of the energy is radiated as discrete-photon radiation by ultra-relativistic particles ($\hbar\omega > 20$ keV) shown in blue, while the classical radiation from mildly relativistic particles ($\gamma \ll 10$) shown in pink line remains insignificant. After the magnetic flux is exhausted, the magnetic and kinetic energies reach equipartition. In Fig. 2(d) we compare pair production efficiency between two strong-field ($B_0 = 2\times10^{11}$ G) runs with different system sizes, $L_y = 277d_e$ and $L_y = 831d_e$. This panel shows that pair production begins to occur in run #1, although the secondary pairs created only represent a small percentage of the pairs composing the initial plasma. For the larger system size run #4 ($L_y/d_e = 831$), where the parameter χ is able to reach larger values, one observes a steep rise of secondary pairs and significantly more pairs are produced.

In Fig. 3 (run #1, $L_y/d_e = 277$) and Fig. 4 (run #4, $L_y/d_e = 831$) we show single-snapshot (at $t = 1050\omega_p^{-1}$) color maps of three quantities: in-plane magnetic field strength (top panels), plasma density (middle panels), and photon number density for the two strong-field simulations. For run #1, $L_y/d_e = 277$, we only show the number density of photons with $\hbar\omega > 0.035 m_e c^2$(20 keV) because these photons represent more than 99.9% of the discrete photon energy. In the case of run #4, $L_y/d_e = 831$, due to computation constraints, we have only shown the number density of hard gamma-rays (photons with $\hbar\omega > 2m_e c^2$(1 MeV)).

In Fig. 3 (run #1, $L_y/d_e = 277$), the maximum magnetic field inside a plasmoid is about twice the initial upstream magnetic field, while in Fig. 3 (run #4, $L_y/d_e = 831$), this ratio goes up to almost twenty. A possible reason behind such a discrepancy is that in run #1, the free energy in the upstream magnetic field runs out before the magnetic field in the island reaches such value. This substantial rise in the magnetic field of the plasmoid aids to increase the gamma-rays density as well as their energy. It is important to note that the emission of hard photons takes place around the magnetic islands where the heating and acceleration of particles is expected to occur.

For a gamma ray to decay into a pair, the characteristic decay length of the gamma ray must be comparable with the characteristic size of a patch of intense magnetic field. However, only photons with $\chi_\gamma \gtrsim 1$ can decay in a pair because the probability is exponentially suppressed for low values of χ as shown in Eq. (10). The characteristic decay length is defined as $l_{decay} = c(dP/dt)^{-1}$, where dP/dt is the probability rate from Eq. (10). When $\chi_\gamma \gtrsim 1$, one can show that $l_{decay} \sim 2000\ c/\Omega_{ce}$ ($\Omega_{ce} \equiv eB/m_e c$ is the cyclotron frequency). In the units of the simulations the normalized characteristic decay length reads $l_{decay}/d_e \sim 2000\ \omega_p/\Omega_{ce}$. For run #1 and run # 4, magnetic islands typically have a size $L/d_e \gtrsim 100$ (see Fig. 3 and Fig. 4) with nearly uniform magnetic fields ($eB/m_e\omega_p c$) of 7 and 20 respectively. These magnetic fields correspond to a characteristic decay length of 285 and 100 respectively which is on the order of the island size. In order to reach $\chi_\gamma \sim 1$, one needs for #1 to have hard photons with energy above $140m_e c^2$ and for #4, hard photons with energy above $50m_e c^2$. In Fig. 1(e) it is shown that hard photons do exist at this limit.

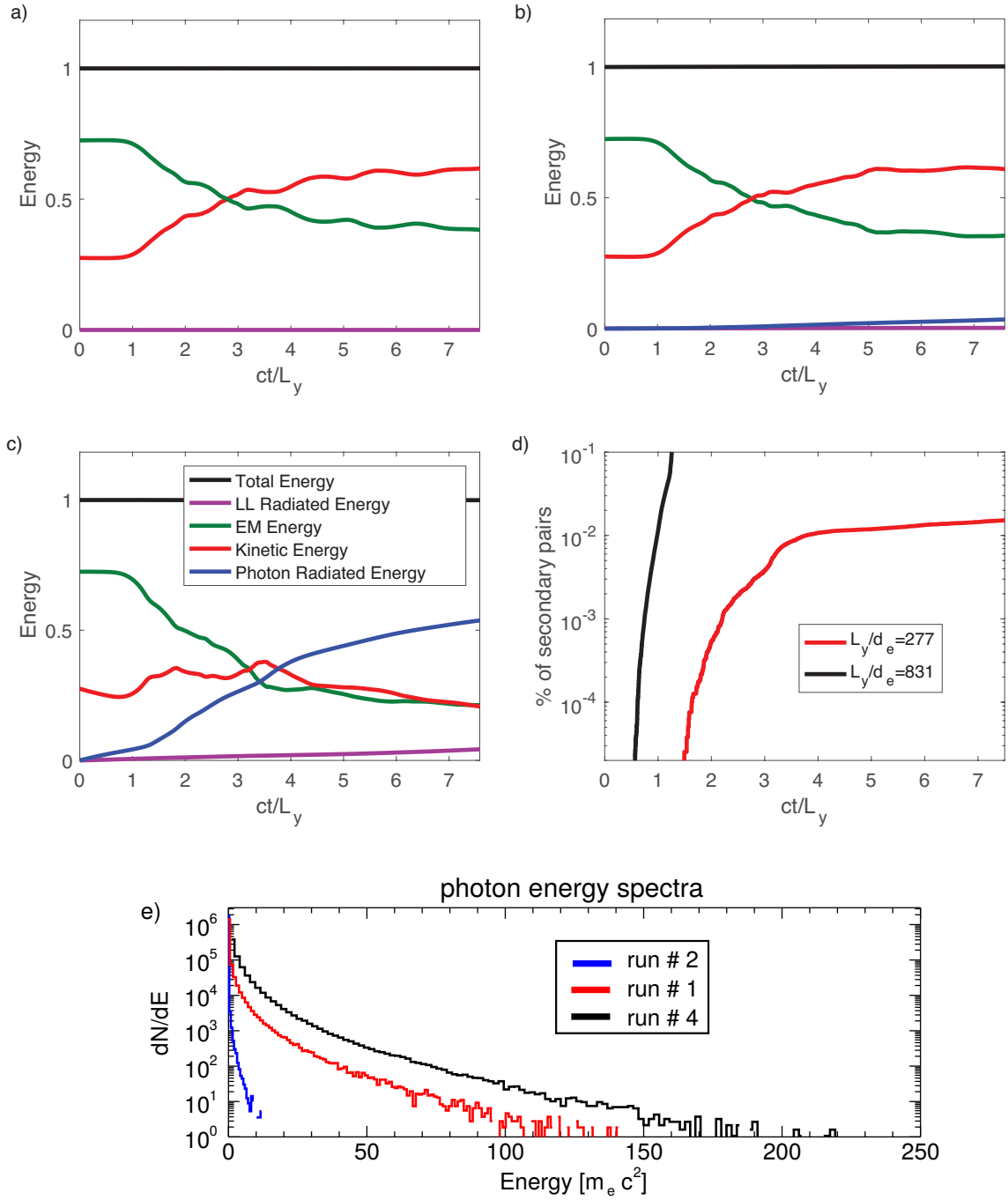

FIG. 2: a)-b)-c) time evolution of the distribution of energy for run #3,#2 and # 1 respectively. d) percentage of secondary pairs created as a function of time for run #1 and #4. e) photon energy spectra for runs #1 #2 and #4 at $t = 1050\ \omega_p^{-1}$ (run # 3 does not emit significant energy photons)

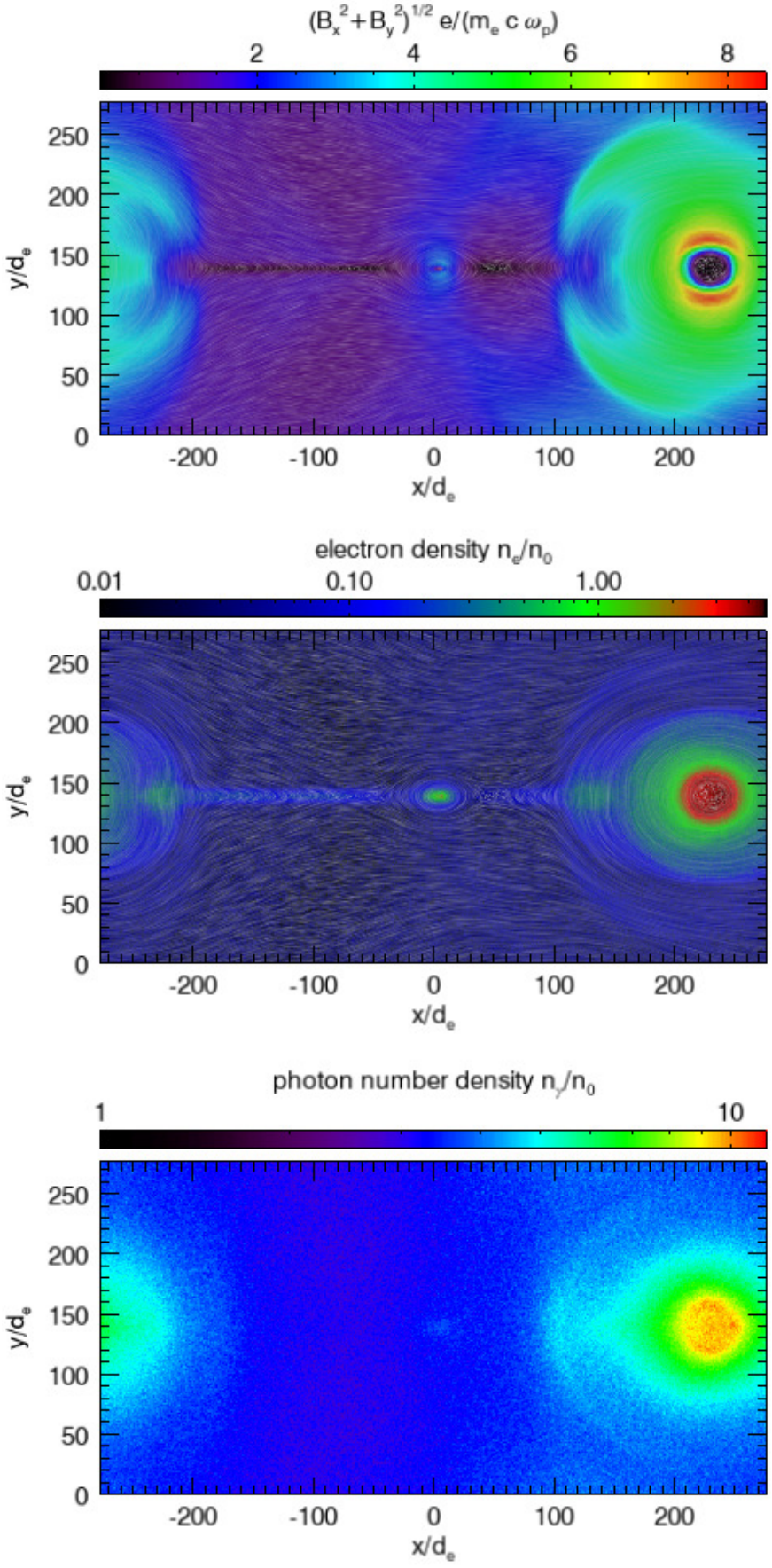

FIG. 3: Top: magnitude of the in-plane magnetic field ; center: positron density in color scale with a white overlay representing the magnetic field lines; bottom: the soft gamma ray ($\hbar\omega > 20$ keV) density. All plots are done for run #1 at $t = 1050\ \omega_p^{-1} = 3.8\ L_y/c$.

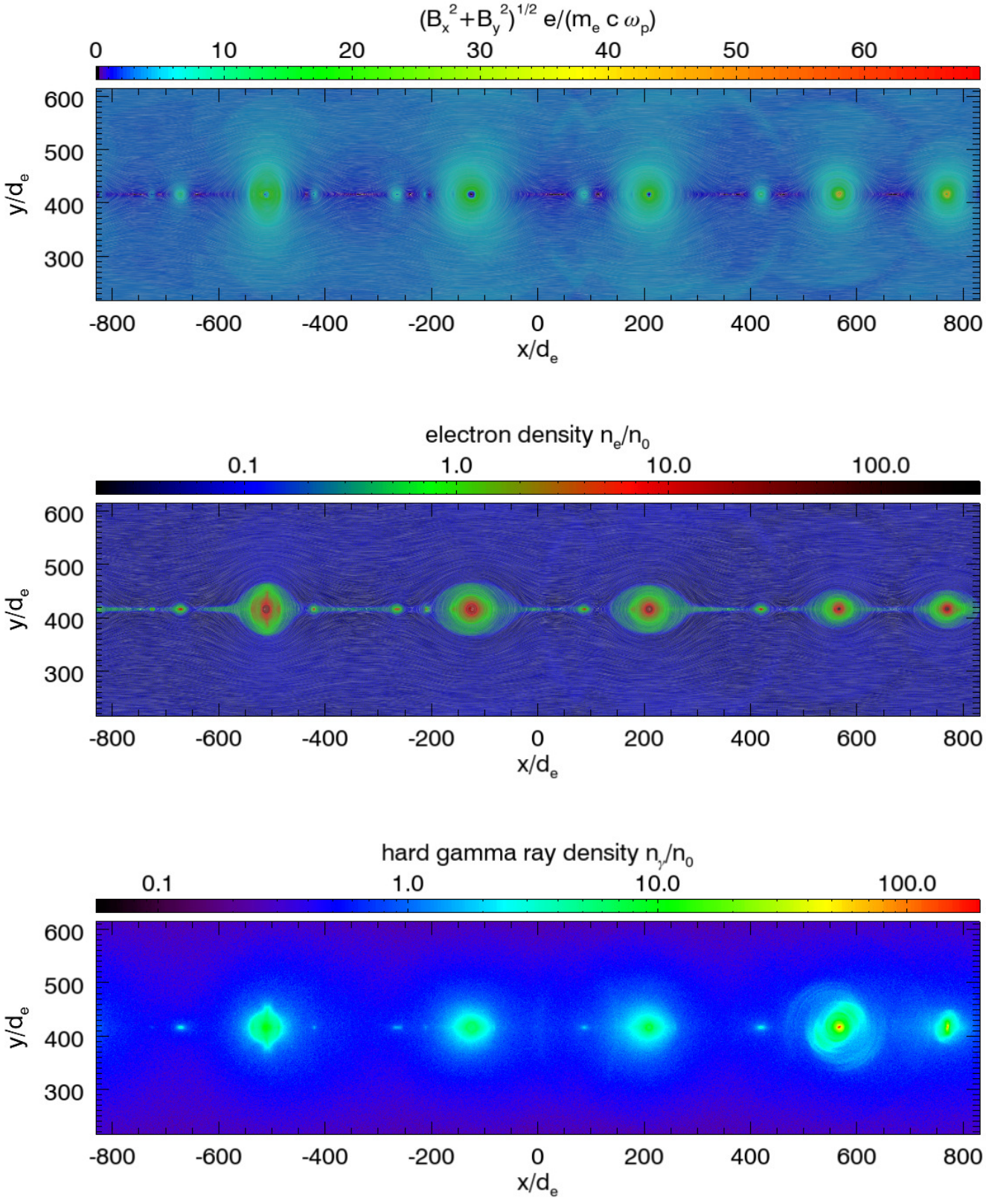

FIG. 4: Top: magnitude of the in-plane magnetic field ; center: positron density in color scale with a white overlay representing the magnetic field lines; bottom: the hard gamma ray ($\hbar\omega > 2m_e c^2$) density. All plots are done for run #4 at $t = 1050\ \omega_p^{-1} = 1.3\ L_y/c$.

IV. CONCLUSIONS

These preliminary results constitute the first numerical study of magnetic reconnection in strong fields where QED effects are self-consistently included from first-principles. We have performed QED-PIC simulations of a relativistic Harris equilibrium immersed in a background pair plasma for increasingly large values of magnetic field. When the value of the magnetic field approaches the critical Schwinger field, the magnetic energy is transferred into radiation rather than into particle kinetic energy. For large system size the magnetic field strength inside an island can be an order of magnitude higher than the upstream magnetic field. This strong field, along with large scale islands, gives rise to abundant hard gamma-rays emission and electron-positron pair production. The mechanism of strong magnetic field enhancement within the islands is not discussed in this document due to its complexity and is reserved for a detailed future publication. This study is a first concrete step towards better understanding of magnetic reconnection as a possible mechanism powering gamma-ray flares in magnetar magnetospheres.

Acknowledgments

This work is supported by the European Research Council (ERC-2015-AdG Grant 695088), FCT (Portugal) Grants SFRH/IF/01780/2013. D. A. Uzdensky gratefully acknowledges the hospitality of the Institute for Advanced Study and support from the Ambrose Monell Foundation. This work was also supported by DOE grant DE-SC0008409, NASA grant NNX16AB28G, and NSF grant AST-1411879. We acknowledge PRACE for awarding access to resource SuperMUC based in Germany at Leibniz research center. Simulations were performed at the Accelerates cluster (Lisbon, Portugal), and SuperMUC (Germany).

V. APPENDIX

A. QED DIFFERENTIAL PROBABILITY RATES

The χ parameter determines if classical or QED interactions dominate the physics and is defined using the 4-momentum p^μ of the particle (electron/positron, or photon):

$$\chi = \frac{\sqrt{(p_\mu F^{\mu\nu})^2}}{B_Q\ mc}. \tag{5}$$

For electrons/positrons, we can also express χ_e as a function of 3-vectors and the background electric and magnetic field vectors:

$$\chi_e = \frac{1}{B_Q}\sqrt{\left(\gamma\vec{E} + \frac{\vec{p}}{mc}\times\vec{B}\right)^2 - \left(\frac{\vec{p}}{mc}\cdot\vec{E}\right)^2}. \tag{6}$$

The differential probability rate of photon emission by nonlinear Compton scattering is then given [4–8] by

$$\frac{d^2P}{dt\ d\chi_\gamma} = \frac{\alpha mc^2}{\sqrt{3}\pi\hbar\gamma\chi_e}\left[\left(1-\xi+\frac{1}{1-\xi}\right)K_{2/3}(\tilde{\chi}) - \int_{\tilde{\chi}}^{\infty} dx K_{1/3}(x)\right], \tag{7}$$

where $\tilde{\chi} = 2\xi/(3\chi_e(1-\xi))$, χ_γ is the χ for the emitted photons, and $\xi = \chi_\gamma/\chi_e$. The total radiated power is

$$P_{rad} = -\int d\epsilon_\gamma\ \epsilon_\gamma \frac{d^2P}{dt\ d\epsilon_\gamma} = -\frac{\epsilon_e}{\chi_e}\int d\chi_\gamma\ \chi_\gamma \frac{d^2P}{dt\ d\chi_\gamma} \tag{8}$$

where $\epsilon_e = \gamma mc^2$ is the electron energy, $\epsilon_\gamma = \hbar\omega$ is the radiated photon energy, and the integration is over all possible photon energies. For $\xi \ll 1$, P_{rad} given by Eq. (8) reduces to the classical Synchrotron radiated power. The differential rate of pair production by a photon in a background electromagnetic field is given [4–8] by

$$\frac{d^2P}{dt\ d\chi_e} = \frac{\alpha m^2c^4}{\sqrt{3}\pi\hbar^2\omega\chi_\gamma}\left[\left(\frac{\xi^+}{\xi^-}+\frac{\xi^-}{\xi^+}\right)K_{2/3}(\tilde{\chi}) + \int_{\tilde{\chi}}^{\infty} dx K_{1/3}(x)\right] \tag{9}$$

where $\tilde{\chi} = 2/(3\chi_\gamma\ \xi^+\xi^-)$ and $\xi^+ = \chi_e/\chi_\gamma = 1 - \xi^-$. The total rate for this process can be approximated for very small or very high χ_γ in the following way:

$$\frac{dP}{dt} = \int d\chi_e \frac{d^2P}{dt\ d\chi_e} \propto \begin{cases} \frac{\alpha m^2 c^4}{\hbar^2 \omega} \chi_\gamma^{2/3}, & \chi_\gamma \gg 1 \\ \exp\left(-\frac{8}{3\chi_\gamma}\right), & \chi_\gamma \ll 1. \end{cases} \tag{10}$$

The aforementioned probabilities are derived in the limit of ultra-relativistic particles. For mildly relativistic particles ($\gamma < 10$), instead of quantum recoil, we take into account radiation reaction using the classical relativistic Landau-Lifshitz formula [15].

[1] D. A. Uzdensky, Magnetic Reconnection: Concepts and Applications **427**, 473 (2016), 1510.05397.
[2] M. Lyutikov, Monthly Notices of the Royal Astronomical Society **346**, 540 (2003).
[3] D. A. Uzdensky, Space Science Reviews **160**, 45 (2011), ISSN 1572-9672.
[4] A. I. Nikishov and V. I. Ritus, Sov. Phys. JETP **19**, 529 (1964).
[5] A. I. Nikishov and V. I. Ritus, Sov. Phys. JETP **25** (1967).
[6] V. Baier and V. Katkov, Physics Letters A **25**, 492 (1967), ISSN 0375-9601.
[7] N. P. Klepikov, Zhur. Esptl. i Teoret. Fiz. **26** (1954).
[8] T. Erber, Rev. Mod. Phys. **38**, 626 (1966).
[9] E. G. Harris, Il Nuovo Cimento (1955-1965) **23**, 115 (1962), ISSN 1827-6121.
[10] C. H. Jaroschek and M. Hoshino, Phys. Rev. Lett. **103**, 075002 (2009).
[11] L. Sironi and A. Spitkovsky, The Astrophysical Journal Letters **783**, L21 (2014).
[12] R. A. Fonseca, L. O. Silva, F. S. Tsung, V. K. Decyk, W. Lu, C. Ren, W. B. Mori, S. Deng, S. Lee, T. Katsouleas, et al., *OSIRIS: A three-dimensional, fully relativistic particle in cell code for modeling plasma based accelerators*, vol. 2331 (Springer Berlin / Heidelberg, 2002).
[13] T. Grismayer, M. Vranic, J. L. Martins, R. A. Fonseca, and L. O. Silva, Physics of Plasmas **23**, 056706 (2016).
[14] T. Grismayer, M. Vranic, J. L. Martins, R. A. Fonseca, and L. O. Silva, Phys. Rev. E **95**, 023210 (2017).
[15] M. Vranic, J. Martins, R. Fonseca, and L. Silva, Computer Physics Communications **204**, 141 (2016), ISSN 0010-4655.